The Journal of Immunology

Activation of Protein Tyrosine Phosphatase Receptor Type γ Suppresses Mechanisms of Adhesion and Survival in Chronic Lymphocytic Leukemia Cells

Alessio Montresor, Lara Toffali, Laura Fumagalli, Gabriela Constantin, Antonella Rigo, Isacco Ferrarini, Fabrizio Vinante and Carlo Laudanna

J Immunol 2021; 207:671-684; Prepublished online 23 June 2021;
doi: 10.4049/jimmunol.2001462
http://www.jimmunol.org/content/207/2/671

The Journal of Immunology is published twice each month by
The American Association of Immunologists, Inc.,
1451 Rockville Pike, Suite 650, Rockville, MD 20852

Print ISSN: 0022-1767 Online ISSN: 1550-6606.

Activation of Protein Tyrosine Phosphatase Receptor Type γ Suppresses Mechanisms of Adhesion and Survival in Chronic Lymphocytic Leukemia Cells

Alessio Montresor,* Lara Toffali,* Laura Fumagalli,* Gabriela Constantin,† Antonella Rigo,‡ Isacco Ferrarini,‡ Fabrizio Vinante,‡ and Carlo Laudanna*

The regulatory role of protein tyrosine kinases in β_1- and β_2-integrin activation and in the survival of chronic lymphocytic leukemia (CLL) cells is well established. In contrast, the involvement of protein tyrosine phosphatases in CLL biology was less investigated. We show that selective activation of the protein tyrosine phosphatase receptor type γ (PTPRG) strongly suppresses integrin activation and survival in leukemic B cells isolated from patients with CLL. Activation of PTPRG specifically inhibits CXCR4- as well as BCR-induced triggering of LFA-1 and VLA-4 integrins and mediated rapid adhesion. Triggering of LFA-1 affinity is also prevented by PTPRG activity. Analysis of signaling mechanisms shows that activation of PTPRG blocks chemokine-induced triggering of JAK2 and Bruton's tyrosine kinase protein tyrosine kinases and of the small GTP-binding protein RhoA. Furthermore, activated PTPRG triggers rapid and robust caspase-3/7–mediated apoptosis in CLL cells in a manner quantitatively comparable to the Bruton's tyrosine kinase inhibitor ibrutinib. However, in contrast to ibrutinib, PTPRG-triggered apoptosis is insensitive to prosurvival signals generated by CXCR4 and BCR signaling. Importantly, PTPRG activation does not trigger apoptosis in healthy B lymphocytes. The data show that activated PTPRG inhibits, at once, the signaling pathways controlling adhesion and survival of CLL cells, thus emerging as a negative regulator of CLL pathogenesis. These findings suggest that pharmacological potentiation of PTPRG tyrosine-phosphatase enzymatic activity could represent a novel approach to CLL treatment. ***The Journal of Immunology*****, 2021, 207: 671–684.**

Chronic lymphocytic leukemia (CLL) is a common, highly heterogeneous leukemia characterized by the clonal expansion of mature, CD5-positive B lymphocytes in the bone marrow (BM), blood, lymph nodes, and spleen (1). In contrast to healthy B lymphocytes, CLL cells have a prolonged life span in BM and lymphoid tissues, where they profit from the stromal microenvironment to avoid apoptosis and undergo uncontrolled accumulation. Among several stromal factors, chemokines play a central role in dissemination and survival of CLL cells, thus favoring the accumulation and permanence of a reservoir of leukemic cells in the BM stromal niches. Accordingly, CLL cells are characterized by higher expression of the CXCL12 chemokine receptor CXCR4 and of β_1-integrin VLA-4, which is a CLL-negative prognostic marker (2, 3). In the context of signaling mechanisms involved in CLL pathogenesis, the protein tyrosine kinase (PTK) Bruton's tyrosine kinase (BTK) plays a critical role (4, 5). BTK couples Ag-activated BCR to downstream signaling (6), involving the activity of PLCG2 (7, 8), in turn triggering protein kinase Cβ (9) and the subsequent activation of MAPKs (10) and NF-κB (11). Moreover, BTK is a downstream effector of classical chemoattractants (12) and chemokine receptors (13–15), leading to activation of MAPKs and PLCG2, the latter having a main role in B cell migration (16). Notably, few phosphatases have also been implicated in CLL pathogenesis. The protein tyrosine phosphatase receptor (PTPR) type O Tyr-phosphatase was shown to interfere with CLL progression and survival and was proposed as a tumor suppressor gene (17). Moreover, it was reported that PHLPP1 and phosphatase-2A Ser/Thr-phosphatases are downmodulated in CLL, thus favoring prosurvival signals in CLL (18, 19). Moreover, SHIP1 and SHIP2 5-phosphate phosphatases have been shown to interfere with prosurvival signaling mechanisms in CLL (20, 21).

Chemokines activate integrins by triggering a complex signal transduction cascade involving at least 77 signaling molecules, mediating rapid integrin affinity and valency upregulation, leading to increased leukocyte adhesiveness (22). Recently, we have demonstrated that in CLL cells, JAK2 and BTK PTKs have a pivotal role in CXCR4-triggered signaling by mediating the activation of the rho-rap module of integrin affinity triggering, ultimately controlling LFA-1– and VLA-4–mediated rapid adhesion (23, 24). Importantly, we showed that BTK activation by CXCR4 is mediated by both JAK2 and heterotrimeric G-protein signaling, whereas, in contrast, BTK activation by BCR relies on JAK2 (24). Thus, JAK2 and BTK PTKs play a concurrent regulatory role in chemokine and BCR signaling in CLL cells. In this context, the counterbalancing activity of PTPs remains poorly defined.

*Department of Medicine, Section of General Pathology, Laboratory of Cell Trafficking and Signal Transduction, University of Verona, Verona, Italy; †Department of Medicine, Section of General Pathology, Laboratory of Neuroimmunology and Neuroinflammation, University of Verona, Verona, Italy; and ‡Department of Medicine, Section of Hematology, Cancer Research and Cell Biology Laboratory, University of Verona, Verona, Italy

ORCIDs: 0000-0002-3855-6747 (F.V.); 0000-0003-4050-1056 (C.L.).

Received for publication December 29, 2020. Accepted for publication May 4, 2021.

This work was supported by the Associazione Italiana per la Ricerca sul Cancro (IG-16797), the Fondazione Fibrosi Cistica (FFC Grant 13/2019), Fondo Unico per la Ricerca, Department of Medicine, University of Verona, and the H2020 European Research Council (Grant 695714 IMMUNOALZHEIMER to G.C.).

Address correspondence and reprint requests to Prof. Carlo Laudanna, Department of Medicine, Section of General Pathology, Laboratory of Cell Trafficking and Signal Transduction, University of Verona, Strada Le Grazie 8, Verona 37134, Italy. E-mail address: carlo.laudanna@univr.it

The online version of this article contains supplemental material.

Abbreviations used in this article: BM, bone marrow; BTK, Bruton's tyrosine kinase; CLL, chronic lymphocytic leukemia; CPP, cell-penetrating peptide; P1-WD, penetratin-1-wedge domain; pNPP, *p*-nitrophenyl phosphate; PTK, protein tyrosine kinase; PTP, protein tyrosine phosphatase; PTPRG, protein tyrosine phosphatase receptor type γ; RS, Richter syndrome; TAT-ICD, TAT-intracellular domain fusion protein.

www.jimmunol.org/cgi/doi/10.4049/jimmunol.2001462

The PTP family includes receptor-like and nontransmembrane proteins, for a total of 38 coding genes (25, 26). We have recently demonstrated in human monocytes the negative regulatory role of PTPR type γ (PTPRG) in chemoattractant-induced integrin activation (27). Consistent with the negative role of PTPRG on integrin triggering, high-throughput phosphoproteomics analysis showed that, among others, JAK2 and BTK PTKs are PTPRG targets of Tyr-dephosphorylation and inhibition (27). Thus, these data suggest that PTPRG could also have a role in CLL. However, the expression and regulatory role of PTPRG in CLL cells have never been studied.

To study PTPRG in primary B cells and to identify possible CLL-specific mechanisms, we analyzed leukemic cells isolated from patients with CLL comparted to B lymphocytes isolated from healthy donors by taking advantage of two complementary approaches we previously developed, based on cell-penetrating peptides (CPPs) and allowing selective activation of PTPRG in primary cells (27). We show that PTPRG activation specifically blocks both CXCR4- and BCR-triggered integrin-mediated static adhesion to ICAM-1 and VCAM-1. The negative role of PTPRG on chemokine signaling was also confirmed in underflow adhesion assays in physiological shear stress conditions. Importantly, PTPRG activation completely inhibited LFA-1 conformational transition to low-intermediate and high-affinity states, both critical to underflow arrest. Analysis of signaling mechanisms shows that PTPRG activation prevents Tyr-phosphorylation and activation of JAK2 and BTK. Moreover, and consistent with integrin LFA-1 affinity downmodulation, PTPRG activity prevents CXCL12-triggered activation of the small GTPase RhoA. Furthermore, we found that activation of PTPRG triggers rapid and robust increase of caspase-3/7 activity in a time- and dose-dependent manner in CLL cells, but not in healthy B lymphocytes, consistent with a CLL-specific PTPRG-mediated proapoptotic effect. Importantly, PTPRG-triggered apoptosis is minimally sensitive to prosurvival signals generated by CXCR4 and BCR engagement. Taken together, our data show that PTPRG activation strongly impairs signaling mechanisms controlling adhesion and survival of CLL cells. These findings are, thus, consistent with a contrasting role of PTPRG on CLL pathogenesis. The data suggest the rationale for the development of novel CLL treatments based on selective pharmacological potentiation of PTPRG Tyr-phosphatase activity.

Materials and Methods

Reagents

Human E-selectin/Fc (catalog number ADP1), human ICAM-1/Fc (catalog number 720-IC), human VCAM-1/Fc (catalog number 862-VC), and human CXCL12 (catalog number 350-NS) were from R&D Systems (Minneapolis, MN); FITC goat secondary Ab to mouse was from Sigma-Aldrich (catalog number F2012; St. Louis, MO); TAT, penetratin-1 (P1), and P1-wedge domain (P1-WD) were synthesized by GenScript (Piscataway, NJ); mAb anti-PTPRG (TPγ B9-2) was kindly provided by Prof. Sorio (University of Verona); KIM127 mouse mAb was from American Type Culture Collection (Rockville, MD); 327A mouse mAb was kindly provided by Dr. Kristine Kikly (Eli Lilly and Company, Indianapolis, IN); goat $F(ab')_2$ anti-human IgM was from SouthernBiotech (catalog number 2022-14; Birmingham, AL); PE anti-human CD184 (CXCR4) was from BioLegend (clone 12G5; catalog number 306505; San Diego, CA); PMA was from Sigma-Aldrich (catalog number P8139); JAK2 (Phospho) [pY1007/pY1008] Human ELISA Kit was from Thermo Fisher Scientific (catalog number KHO5621; Waltham, MA); PE mouse anti-BTK (pY223) Ab was from BD Biosciences (catalog number 562753; San Jose, CA); RhoA G-LISA activation assay Kit was from Cytoskeleton (catalog number BK124; Denver, CO); and CellEvent Caspase-3/7 Green Assay Kit was from Thermo Fisher Scientific (catalog number C10427).

Isolation of B lymphocytes from healthy subjects and patients with CLL

Normal and CLL B lymphocytes were isolated from PBMCs after blood separation on Ficoll-Paque Plus and purification by negative selection (Miltenyi Biotec). Purity of B lymphocyte preparations was checked by flow cytometry with anti-CD19 mAb (BD Biosciences). The study involved a total of 21 patients with a diagnosis of CLL compared with normal B lymphocytes isolated from healthy donors. The diagnosis of CLL was made upon clinical and laboratory parameters at the hematology section of the Department of Clinical and Experimental Medicine, University of Verona. Patients with CLL have been selected for complete absence of any previous treatment. Blood samples were obtained in the context of the project 1828/2010 approved by the ethics committee of Verona University Hospital; written informed consent was obtained according to Italian law. Blood samples from patients with CLL contained CD5-positive cells ranging from 70 to 96% with an average of 86 ± 7% (Table I).

Trojan CPP technology

The control TAT and P1 and the fusion P1-WD peptides were synthesized by GenScript. The P1-WD peptide (RQIKIWFQNRRMKWKKGKQFV KHIGELYSNNQHGFSEDFEEVQ) encompassed the complete P1 sequence (16 aa; RQIKIWFQNRRMKWKK), an inserted glycine to allow flexibility of the fusion peptide, and the previously identified, 26-aa–long, PTPRG WD sequence encompassing aa 831 to 856 of human PTPRG (KQFVKHIGELYSNNQHGFSEDFEEVQ) (27). PTPRG TAT-intracellular domain (TAT-ICD) fusion protein was generated by using the pRSET-TATa expression vector, as reported (27). Concentrated stock samples of purified native TAT-ICD fusion protein were stored at −20°C. The tyrosine phosphatase activity of the TAT-ICD preparations was systematically quantified by means of a *p*-nitrophenyl phosphate (pNPP) assay. Freshly purified TAT-ICD was dissolved in pNPP assay buffer (20 mM Tris, 10 mM DTT, and 2 mM pNPP) in the presence or absence of orthovanadate, and the dephosphorylating activity was evaluated, after 30 min of incubation, at 405 nm by a plate reader. See YouTube animations at https://www.youtube.com/watch?v=wf8VF6SQaHo for the mechanisms of action of P1-WD and TAT-ICD CPPs.

Static adhesion assay

B lymphocytes were suspended in standard adhesion buffer (PBS plus 10% FBS plus Ca^{2+} 1 mM plus Mg^{2+} 1 mM [pH 7.2]). Adhesion assays were performed on 18-well glass slides coated with human ICAM-1 or VCAM-1, 1 μg/ml in PBS. A total of 20 μl of cell suspension was added to the well and stimulated at 37°C with 5 μl of CXCL12, 0.5 μM final concentration, for 120 s, or with 5 μl of PMA, 50 ng/ml final concentration, for 10 min. After washing, adherent cells were fixed in 1.5% glutaraldehyde in ice-cold PBS and counted by computer-assisted enumeration, as previously reported (27).

Underflow adhesion assay

Cell behavior in underflow conditions was studied with the BioFlux 200 system (Fluxion Biosciences, South San Francisco, CA). The 48-well plate microfluidics were first coated overnight at room temperature with 2.5 μg/ml human E-selectin together with 10 μg/ml human ICAM-1 or with VCAM-1 alone in PBS. Before use, microfluidic channels were washed with PBS and then coated with 4 μM CXCL12 in PBS for 3 h at room temperature, and the assay was done at wall shear stress of 1 dyne/cm^2. The behavior of interacting lymphocytes was recorded on a digital drive with a fast CCD camera (25 frames/s, capable of 1/2 subframe 20-ms recording) and analyzed subframe by subframe. Single areas of 0.2 mm^2 were recorded for at least 60 s. Interactions of ≥20 ms were considered significant and scored. Lymphocytes that remained firmly adherent for at least 10 s, thus including also events of adhesion stabilization, were considered fully arrested and scored. Rolling interacting and arrested cell behaviors were automatically detected and quantified with BeQuanti.

Measurement of LFA-1 affinity states

B lymphocytes were briefly preincubated with 10 μg/ml of KIM127 or 327A mAbs and stimulated under stirring conditions for 120 s with 0.5 μM CXCL12 at 37°C. After rapid washing, cells were stained by FITC secondary polyclonal Ab and analyzed by flow cytometer (MACSQuant Analyzer 10; Miltenyi Biotec). The acquisition gate was restricted to lymphocyte gate based on morphological characteristics, and 15,000 lymphocytes were acquired and analyzed.

BTK activation

BTK activation was measured by means of tyrosine 223 phosphorylation. Cells were treated and stimulated as indicated and, after a rapid wash, fixed

in formaldehyde 4% for 30 min at 4°C. Cells were washed and suspended in permeabilization buffer (PBS plus 5% FBS plus 0.5% saponin) containing PE-conjugated anti–pY223-BTK Ab for 30 min at 4°C. Cells were washed, suspended in ice-cold PBS, and analyzed by cytofluorimetric quantification. The acquisition gate was restricted to lymphocyte gate based on morphological characteristics, and 15,000 lymphocytes were acquired and analyzed.

JAK2 activation

JAK2 activation was measured by ELISA kit (JAK2 pYpY1007/1008; Life Technologies, Carlsbad, CA). Cells were treated and stimulated as indicated and then lysed at 4°C. Cell lysates were tested for pYpY1007/1008 JAK2, and colorimetric signals were detected by a plate reader (Victor X5 Multilabel Plate Reader; PerkinElmer, Waltham, MA).

RhoA activation

RhoA activation was measured by using a commercial kit (G-LISA RhoA Activation Assay Biochem Kit; Cytoskeleton). Cells were treated and stimulated as indicated and then lysed at 4°C. Cell lysates were tested for GTP-loaded RhoA, and colorimetric signals were detected by a plate reader.

Kinetic analysis of apoptosis

Cell apoptosis was evaluated with the CellEvent Caspase-3/7 Green Assay Kit. A total of 10^6 cells/well was dispensed in 24-well plates in the presence or absence of different agonists. Kinetics of increased caspase-3/7 activity were evaluated by time-lapse video microscopy with a Zeiss AxioObserver 7 inverted wide-field microscope, equipped with thermostatic chamber, Colibri 7 fluorescent LED illumination, full motorized stage, Hamamatsu ORCA-Flash4.0 V3 Digital CMOS camera, set at 8 output bit depth, and the Zeiss ZEN 2.6 time-lapse module. The 24-well plates were kept at 37°C in a 5% CO_2 humidified atmosphere; video acquisition was with a 40× Plan Apochromatic objective (numerical aperture 0.65) corresponding to an acquisition area of 1.2×10^5 μm^2, with a cell density of 500 cells/acquisition area. Each field was acquired in bright-field and fluorescent light illumination (503/530-nm excitation/emission). Exposure time for fluorescent light was set at 500 ms and left unchanged for the entire duration of the experiment. Time-lapse imaging was for 24 h, with a 15-min time frame, allowing acquisition of 96 frames/condition. Frame-by-frame image analysis was performed, without image preprocessing, with the Zeiss ZEN 2.6 image analysis module, allowing automatic cell segmentation, recognition, and pixel intensity quantification. Pixel intensity (0–256 gray levels) was linear over time with the intensity of emitted fluorescence, in turn proportional to caspase-3/7 enzymatic activity. A total of 48,000 cellular events/24 h for every condition were analyzed. Fluorescence intensity was normalized to the area of every analyzed cell and expressed as intensity per micrometer squared. Data were either expressed and plotted as number of caspase-3/7–positive cells over time or as individual cell and average fluorescence intensity reached after 24 h.

Flow cytometric detection of cell surface CXCR4 expression

B lymphocytes were treated and stimulated as indicated. After washing, cells were stained with anti-CXCR4 Ab for 1 h at 4°C and analyzed by flow cytometer (MACSQuant Analyzer 10; Miltenyi Biotec). The acquisition gate was restricted to lymphocyte gate based on morphological characteristics, and 15,000 lymphocytes were acquired and analyzed.

Statistical analysis

Results are expressed as mean ± SD. Statistical significance was assessed by Mann–Whitney *U* test or one-way ANOVA followed by post hoc Dunnett multiple-comparisons test at the 95% confidence level (control columns were set at P1 or TAT alone treatment condition). Statistical significance threshold was set at $p < 0.05$ (*$p < 0.05$, **$p < 0.01$, ***$p < 0.001$). All statistical analyses and data plots were performed using GraphPad Prism version 8 software (GraphPad Software).

Results

Activation of PTPRG inhibits signaling mechanisms of integrin triggering in human primary healthy B lymphocytes

By using an mAb selective for the PTPRG extracellular region (TPγ B9-2) (28), we first confirmed that PTPRG is equally expressed on both healthy and CLL B cells (Fig. 1A). Considering the opposite biochemical role of phosphatases with respect to kinases, an effective methodology to study the functional role of protein phosphatases would allow activating the phosphatase activity itself. Notably, PTPRG is normally expressed as a homodimer devoid of enzymatic activity (11). Because monomeric PTPRG has a very high intrinsic enzymatic activity (29), PTPRG can be activated by receptor monomerization. However, physiological activators of PTPRG are unknown. Thus, to investigate the regulatory role of PTPRG in primary cells, we have recently developed the PTPRG-specific P1-WD Trojan peptide (27), which selectively unleashes, by induced receptor monomerization, the intrinsic Tyr-phosphatase activity of PTPRG. We exploited this approach to first evaluate whether activation of PTPRG could inhibit integrin triggering in healthy B lymphocytes.

In static adhesion assays, pretreatment with P1-WD inhibited in a dose-dependent manner CXCL12-induced rapid adhesion to both ICAM-1 (Fig. 1B) and VCAM-1 (Fig. 1C). Furthermore, pretreatment with P1-WD also inhibited BCR-induced adhesion to ICAM-1 (Fig. 1D) and VCAM-1 (Fig. 1E). To corroborate these data, we evaluated the effect of P1-WD on CXCL12-triggered rapid arrest in underflow conditions at physiological shear stress. Pretreatment with P1-WD markedly reduced the percentage of arrested cells both on ICAM-1 and VCAM-1 (Fig. 1F, 1G), with a corresponding increase of rolling cells, as expected. To further characterize the antiadhesive role of PTPRG, we measured LFA-1 heterodimer conformational changes by using two mAbs, recognizing the low-intermediate and high-affinity states of LFA-1 (KIM127 and 327A mAbs, respectively). Pretreatment with P1-WD completely blocked chemokine-triggered transition of LFA-1 to both low-intermediate (Fig. 1H, 1I) and high-affinity states (Fig. 1J, 1K). The P1 control peptide was ineffective in all conditions.

Next, we evaluated whether activation of PTPRG was able to interfere with signaling mechanisms mediating integrin activation. Pretreatment with P1-WD peptide strongly inhibited CXCL12-triggered JAK2 phosphorylation on tyrosine 1007/1008 (Fig. 1L). Moreover, pretreatment with P1-WD inhibited CXCL12-induced BTK phosphorylation on tyrosine-223, a residue critical to BTK kinase activity (12, 16, 30–32) (Fig. 1M, 1N). Furthermore, because the small GTPase RhoA is a downstream effector of both JAK and BTK PTKs and is critically involved in integrin affinity upregulation, we tested whether PTPRG activation was able to prevent RhoA activation by CXCL12. Pretreatment with P1-WD strongly inhibited CXCL12-induced RhoA activation (Fig. 1O). The P1 control peptide was ineffective in all settings.

To confirm these findings with a complementary approach, we generated a Tyr-phosphatase active TAT fusion protein encompassing both the D1 enzymatic and the D2 regulatory intracellular domains of PTPRG. The PTPRG TAT-ICD fusion protein was previously biochemically characterized and demonstrated to translocate into the cell cytosol of primary cells fully retaining the tyrosine phosphatase activity (27). In static adhesion assays, pretreatment of healthy B lymphocytes with TAT-ICD inhibited in a dose-dependent manner CXCL12-induced rapid adhesion to both ICAM-1 (Fig. 2A) and VCAM-1 (Fig. 2B). Furthermore, pretreatment with TAT-ICD also inhibited BCR-induced adhesion to ICAM-1 (Fig. 2C) and VCAM-1 (Fig. 2D). Moreover, in underflow adhesion assays, pretreatment with TAT-ICD markedly reduced the percentage of arrested cells to both ICAM-1 and VCAM-1 (Fig. 2E, 2F). TAT-ICD also completely blocked chemokine-triggered transition of LFA-1 to both low-intermediate (Fig. 2G, 2H) and high-affinity states (Fig. 2I, 2J). Furthermore, TAT-ICD blocked CXCL12-triggered JAK2 (Fig. 2K) and BTK Tyr-phosphorylation (Fig. 2L, 2M), as well as RhoA activation by CXCL12 (Fig. 2N). The TAT control peptide was ineffective in all assays.

Altogether, these data demonstrate that, upon activation, PTPRG becomes a strong negative regulator of signaling mechanisms controlling β_1- and β_2-integrin activation in human primary B lymphocytes.

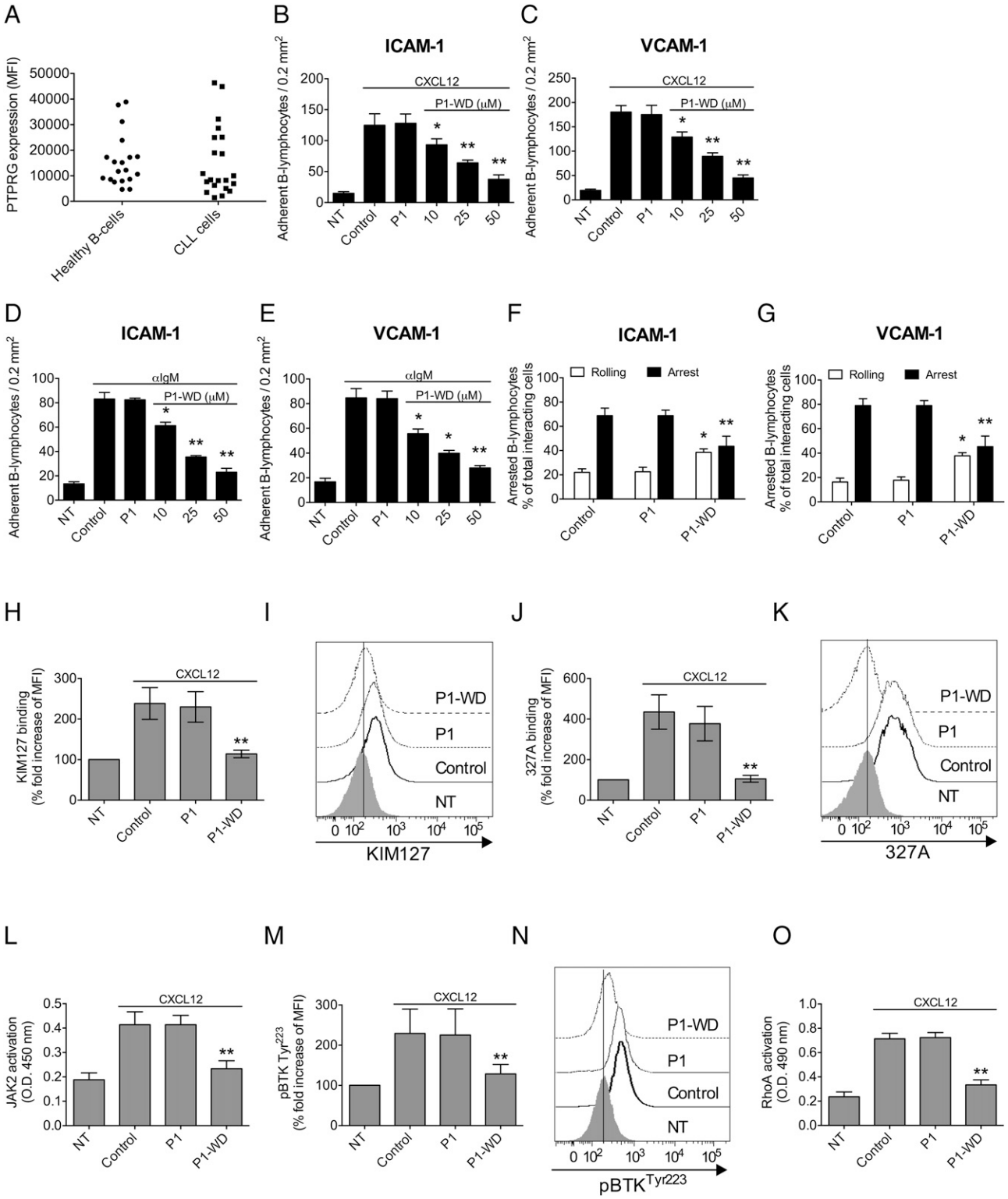

FIGURE 1. Activation of endogenous PTPRG inhibits inside-out signaling to integrin activation and dependent adhesion in healthy B lymphocytes. (**A**) Mean fluorescence of PTPRG staining in healthy (n = 19) and CLL (n = 21) B lymphocytes. (**B**) Static adhesion on ICAM-1 of cells treated with DMSO (not treated [NT] and Control), 50 μM P1, or indicated doses of P1-WD for 1 h at 37°C and then stimulated with CXCL12 500 nM (n = 5, in duplicate). (**C**) Static adhesion on VCAM-1 of cells treated as in (B) (n = 5, in duplicate). (**D**) Static adhesion on ICAM-1 of cells treated as in (B) and stimulated with 10 μg/ml anti-IgM (n = 5, in duplicate). (**E**) Static adhesion on VCAM-1 of cells treated as in (B) and stimulated with 10 μg/ml anti-IgM (n = 5, in duplicate). (**F**) Underflow adhesion on ICAM-1 of cells treated with DMSO (Control), P1, or P1-WD (50 μM) for 1 h at 37°C (n = 4). (**G**) Underflow adhesion on VCAM-1 of cells treated as in (F) (n = 4). (**H**) LFA-1 low-intermediate affinity measurement of cells treated as in (F) and stimulated with 500 nM CXCL12 (n = 4). Shown are the percentages of fold increase over NT. (**I**) Histograms of fluorescence of a representative experiment of LFA-1 low-intermediate affinity. (**J**) LFA-1 high-affinity measurement of cells treated and stimulated as in (F) (n = 4). Shown are the percentages of fold increase over NT. (**K**) Histograms of fluorescence of a representative experiment of LFA-1 high affinity. (**L**) JAK2 activation assay in cells treated and stimulated as in *(Figure legend continues)*

Table I. List of patients with CLL involved in this study

Patient No.	Percentage of CD5/CD19	IgVH	CD38	Age, y (Sex)
1	88	NM	P	74 (male)
2	85	NM	P	83 (male)
3	90	M	N	66 (male)
4	89	M	P	68 (male)
5	78	NM	N	62 (female)
6	90	NM	P	50 (male)
7	84	M	P	70 (male)
8	75	M	N	68 (female)
9	87	M	N	45 (male)
10	90	NM	N	71 (male)
11	85	NM	P	50 (female)
12	70	NM	N	80 (female)
13	92	NM	N	48 (male)
14	85	M	P	74 /male)
15	95	NM	P	53 (male)
16	89	M	N	44 (male)
17	95	NM	N	59 (male)
18	96	NM	N	81 (female)
19	83	NM	N	60 (female)
20	76	M	N	72 (male)
21	95	NM	N	76 (male)

M, mutated; N, negative (<30% on CLL cells); NM, unmutated; P, positive (>30% on CLL cells).

Activation of PTPRG inhibits signaling mechanisms of integrin triggering in CLL cells

We next evaluated the effect of PTPRG activation on integrin-mediated adhesion in CLL cells (Table I). It was of primary interest to test the effect of the P1-WD to exclude that, due to neoplastic progression, the PTPRG intermolecular regulatory WD, which is the target of steric hindrance by P1-WD (27), was not mutated or deleted in CLL cells, thus making PTPRG resistant to triggered monomerization. In static adhesion assays, pretreatment of CLL cells with P1-WD reduced in a dose-dependent manner CXCL12-induced rapid adhesion to both ICAM-1 (Fig. 3A) and VCAM-1 (Fig. 3B). Moreover, similarly to healthy B lymphocytes, pretreatment with P1-WD also inhibited adhesion to ICAM-1 (Fig. 3C) and VCAM-1 (Fig. 3D) triggered by BCR engagement. The P1 control peptide was ineffective. P1-WD was also highly effective in underflow conditions. Indeed, pretreatment with P1-WD significantly reduced the percentage of arrested CLL cells on both ICAM-1 and VCAM-1 (Fig. 3E, 3F), with a corresponding increase of rolling cells. Furthermore, pretreatment with P1-WD almost completely blocked chemokine-triggered transition of LFA-1 to both low-intermediate (Fig. 3G, 3H) and high-affinity states (Fig. 3I, 3J). Analysis of signaling mechanisms confirmed the negative regulatory role of PTPRG on integrin activation by chemokines also in CLL cells. Indeed, pretreatment with P1-WD induced a marked inhibition of CXCL12-triggered JAK2 (Fig. 3K) and BTK (Fig. 3L, 3M) Tyr-phosphorylation. Finally, pretreatment with P1-WD markedly inhibited CXCL12-induced RhoA activation (Fig. 3N). The P1 control peptide was ineffective in all settings. Together, the data show the full responsiveness of CLL cells to P1-WD, indicating that in CLL cells, the regulatory PTPRG WD is conserved and that the D1 enzymatic and the D2 regulatory intracellular domains of PTPRG are functional.

The strong effect of P1-WD on CLL cell adhesion and signaling was then confirmed by exploiting the TAT-ICD–based approach. Pretreatment with TAT-ICD inhibited, in a dose-dependent manner, CXCL12-induced rapid static adhesion to both ICAM-1 (Fig. 4A) and VCAM-1 (Fig. 4B). Furthermore, pretreatment with TAT-ICD also inhibited BCR-induced adhesion to ICAM-1 (Fig. 4C) and VCAM-1 (Fig. 4D). Moreover, in underflow adhesion assays, pretreatment with TAT-ICD consistently reduced the percentage of arrested cells to both ICAM-1 and VCAM-1 (Fig. 4E, 4F). TAT-ICD also completely blocked chemokine-triggered LFA-1 transition to both low-intermediate (Fig. 4G, 4H) and high-affinity states (Fig. 4I, 4J). Analysis of signaling mechanisms fully confirmed the TAT-ICD efficacy. Indeed, pretreatment with TAT-ICD completely inhibited CXCL12-triggered JAK2 (Fig. 4K) and BTK (Fig. 4L, 4M) Tyr-phosphorylation. Finally, pretreatment with TAT-ICD completely prevented RhoA activation by CXCL12 (Fig. 4N). The TAT control peptide was ineffective in all settings.

Altogether, these data show that CLL cells are fully responsive to PTPRG activation, highlighting, for the first time to our knowledge, that PTPRG is a strong negative regulator of signaling mechanisms controlling integrin-mediated adhesion in CLL cells.

PTPRG activation does not affect CXCR4 internalization nor PMA-induced integrin activation

To investigate the functional specificity of PTPRG, we first evaluated whether activated PTPRG could affect the downmodulation of CXCR4 surface expression upon CXCL12 stimulation. In either healthy or CLL B lymphocytes, stimulation with CXCL12 induced a time-dependent downmodulation of CXCR4 expression, as expected (Supplemental Fig. 1A–H, Fig. 5A–H). Pretreatment with P1-WD or with TAT-ICD did not alter the basal expression of CXCR4 (data not shown). Furthermore, pretreatment with P1-WD (Supplemental Fig. 1A–D, Fig. 5A–D) or with TAT-ICD (Supplemental Fig. 1E–H, Fig. 5E–H) did not prevent CXCR4 downmodulation induced by CXCL12 in both healthy and CLL B cells, respectively. As a further test, we studied integrin-mediated adhesion upon PMA stimulation. In healthy as well as in CLL B lymphocytes, pretreatment with P1-WD (Supplemental Fig. 1I, 1J, Fig. 5I, 5J) or with TAT-ICD (Supplemental Fig. 1K, 1L, Fig. 5K, 5L) did not inhibit PMA-triggered static adhesion on ICAM-1 or VCAM-1. Overall, these data support a functional specificity of PTPRG on CXCL12- and BCR-triggered signaling events leading to integrin activation.

Activation of PTPRG triggers robust apoptosis in CLL cells, but not in healthy B lymphocytes

Signals from stromal factors, such as the chemokine CXCL12, are critical to CLL cell survival (33–37). Thus, considering the effect of PTPRG activation on chemokine and BCR signaling, we asked whether, with respect to healthy B lymphocytes, PTPRG activation could affect the survival of CLL cells, both in the absence and presence of stromal factors, by applying a time lapse–based methodology to precisely monitor in real time the kinetics of apoptosis. PTPRG-activating CPPs were compared, as positive control, to the BTK irreversible inhibitor ibrutinib, which we previously showed to also inhibit integrin activation in CLL cells (24).

In healthy B lymphocytes, ibrutinib did not trigger an increase of the number of apoptotic cells with respect to untreated cells. Moreover, with respect to P1 and TAT control peptides, the PTPRG-activating P1-WD peptide and the TAT-ICD fusion protein were unable

(F) ($n = 5$, in duplicate). (**M**) BTK activation assay in cells treated and stimulated as in (F) ($n = 9$). Shown are the percentages of fold increase over NT. (**N**) Histograms of fluorescence of a representative experiment of BTK activation. (**O**) RhoA activation of cells treated and stimulated as in (F) ($n = 5$ in duplicate). All data are expressed as mean ± SD. *$p < 0.05$, **$p < 0.01$ versus P1.

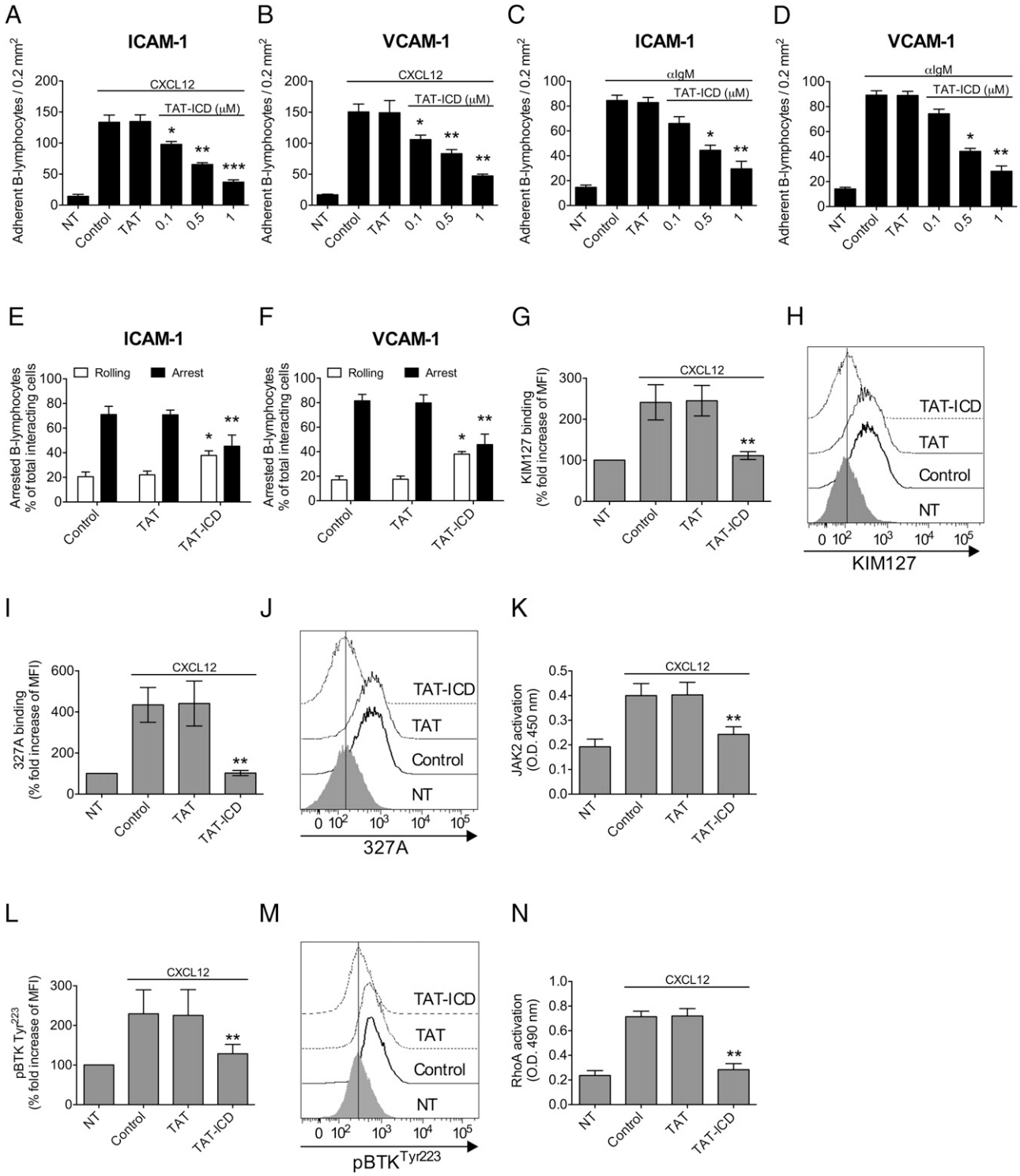

FIGURE 2. A cell-permeable PTPRG active Tyr-phosphatase domain inhibits inside-out signaling to integrin activation and dependent adhesion in healthy B lymphocytes. (**A**) Static adhesion on ICAM-1 of cells treated with DMSO (not treated [NT] and Control), 1 μM TAT, or indicated doses of TAT-ICD for 1 h at 37°C and then stimulated with CXCL12 500 nM ($n = 5$, in duplicate). (**B**) Static adhesion on VCAM-1 of cells treated as in (A) ($n = 5$, in duplicate). (**C**) Static adhesion on ICAM-1 of cells treated as in (A) and stimulated with 10 μg/ml anti-IgM ($n = 5$, in duplicate). (**D**) Static adhesion on VCAM-1 of cells treated as in (A) and stimulated with 10 μg/ml anti-IgM ($n = 5$, in duplicate). (**E**) Underflow adhesion on ICAM-1 of cells treated with DMSO (Control), TAT, or TAT-ICD (1 μM) for 1 h at 37°C ($n = 4$). (**F**) Underflow adhesion on VCAM-1 of cells treated as in (E) ($n = 4$). (**G**) LFA-1 low-intermediate affinity measurement of cells treated as in (E) and stimulated with 500 nM CXCL12 ($n = 4$). Shown are the percentages of fold increase over NT. (**H**) Histograms of fluorescence of a representative experiment of LFA-1 low-intermediate affinity. (**I**) LFA-1 high-affinity measurement of cells treated and stimulated as in (E) ($n = 4$). Shown are the percentages of fold increase over NT. (**J**) Histograms of fluorescence of a representative experiment of LFA-1 high affinity. (**K**) JAK2 activation assay in cells treated and stimulated as in (E) ($n = 5$, in duplicate). (**L**) BTK activation assay in cells treated and stimulated as in (E) ($n = 9$). Shown are the percentages of fold increase over NT. (**M**) Histograms of fluorescence of a representative experiment of BTK activation. (**N**) RhoA activation of cells treated and stimulated as in (E) ($n = 5$ in duplicate). All data are expressed as mean ± SD. $^*p < 0.05$, $^{**}p < 0.01$, $^{***}p < 0.001$ versus TAT.

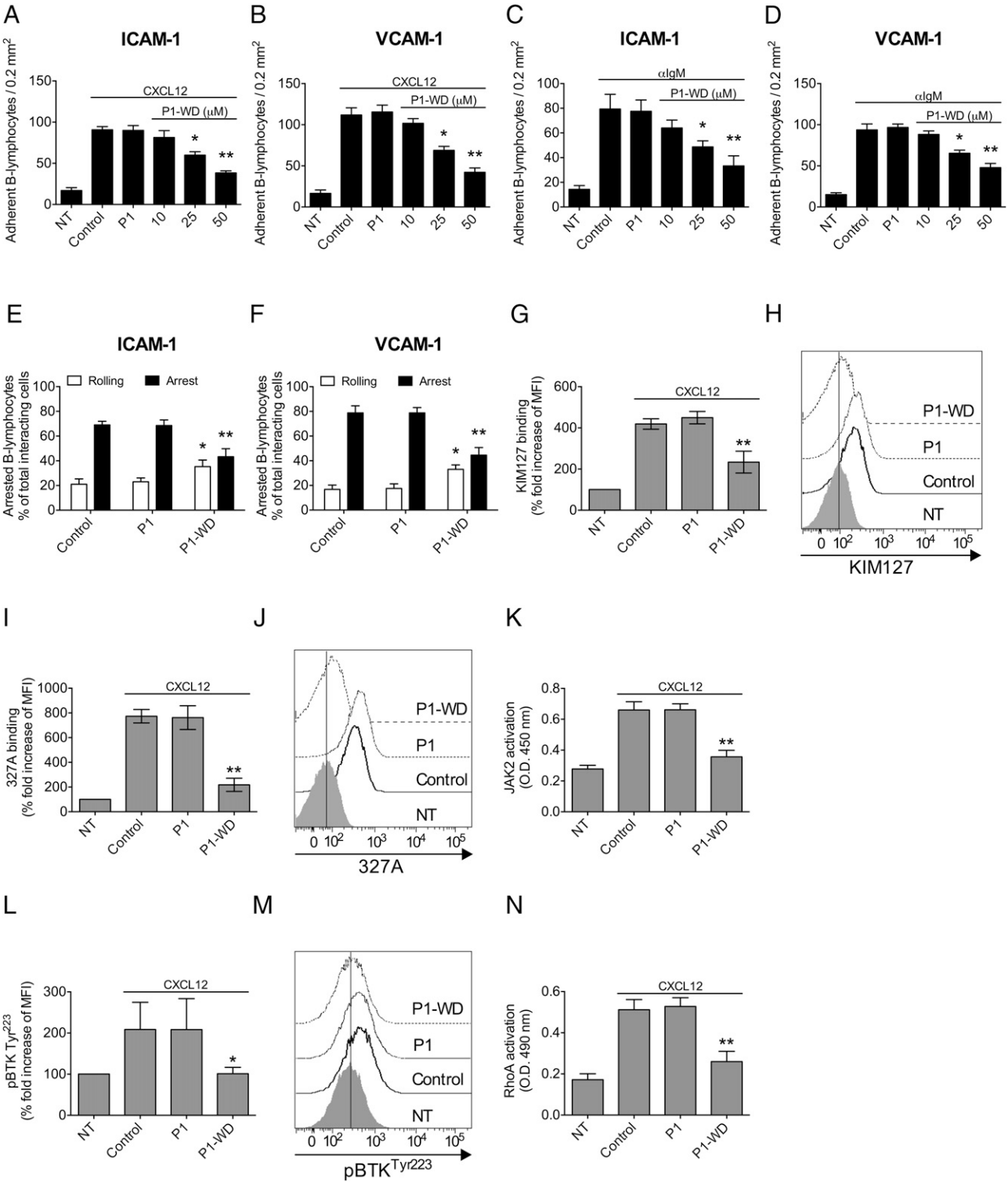

FIGURE 3. Activation of endogenous PTPRG inhibits inside-out signaling to integrin activation and dependent adhesion in CLL B cells. (**A**) Static adhesion on ICAM-1 of cells treated with DMSO (not treated [NT] and Control), 50 μM P1, or indicated doses of P1-WD for 1 h at 37°C and then stimulated with 500 nM CXCL12 ($n = 5$, in duplicate). (**B**) Static adhesion on VCAM-1 of cells treated as in (A) ($n = 5$, in duplicate). (**C**) Static adhesion on ICAM-1 of cells treated as in (A) and stimulated with 10 μg/ml anti-IgM ($n = 5$, in duplicate). (**D**) Static adhesion on VCAM-1 of cells treated as in (A) and stimulated with 10 μg/ml anti-IgM ($n = 5$, in duplicate). (**E**) Underflow adhesion on ICAM-1 of cells treated with DMSO (Control), P1, or P1-WD (50 μM) for 1 h at 37°C ($n = 4$). (**F**) Underflow adhesion on VCAM-1 of cells treated as in (E) ($n = 4$). (**G**) LFA-1 low-intermediate affinity measurement of cells treated as in (E) and stimulated with 500 nM CXCL12 ($n = 3$). Shown are the percentages of fold increase over NT. (**H**) Histograms of fluorescence of a representative experiment of LFA-1 low-intermediate affinity. (**I**) LFA-1 high-affinity measurement of cells treated and stimulated as in (E) ($n = 3$). Shown are the percentages of fold increase over NT. (**J**) Histograms of fluorescence of a representative experiment of LFA-1 high affinity. (**K**) JAK2 activation assay in cells treated and then stimulated as in (E) ($n = 5$, in duplicate). (**L**) BTK activation assay in cells treated and stimulated as in (E) ($n = 5$). Shown are the percentages of fold increase over NT. (**M**) Histograms of fluorescence of a representative experiment of BTK activation. (**N**) RhoA activation of cells treated and stimulated as in (E) ($n = 5$ in duplicate). All data are expressed as mean ± SD. *$p < 0.05$, **$p < 0.01$ versus P1.

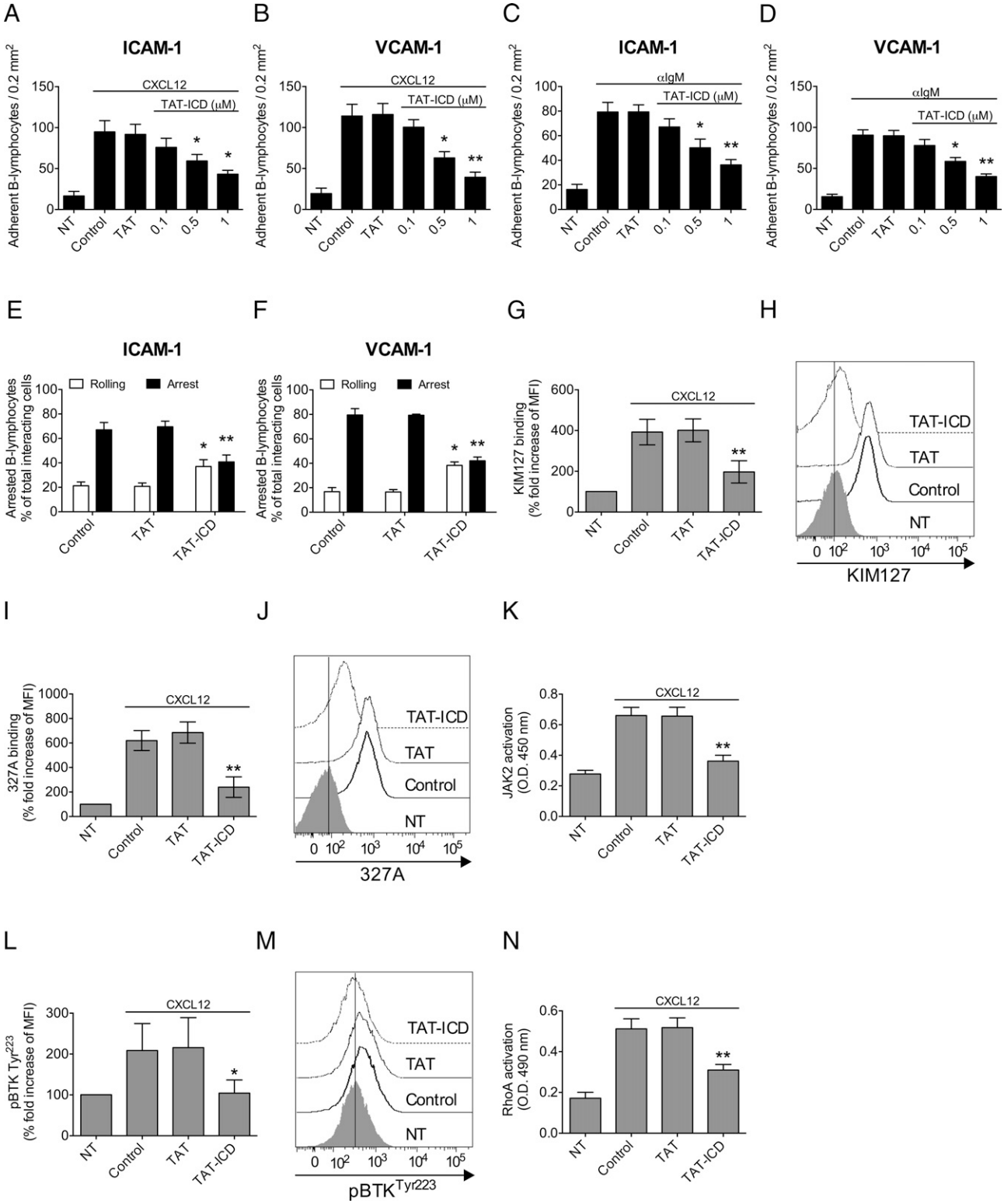

FIGURE 4. A cell-permeable PTPRG active Tyr-phosphatase domain inhibits inside-out signaling to integrin activation and dependent adhesion in CLL B cells. (**A**) Static adhesion on ICAM-1 of cells treated with DMSO (not treated [NT] and Control), 1 μM TAT, or indicated doses of TAT-ICD for 1 h at 37°C and then stimulated with 500 nM CXCL12 ($n = 5$, in duplicate). (**B**) Static adhesion on VCAM-1 of cells treated as in (A) ($n = 5$, in duplicate). (**C**) Static adhesion on ICAM-1 of cells treated as in (A) and stimulated with 10 μg/ml anti-IgM ($n = 5$, in duplicate). (**D**) Static adhesion on VCAM-1 of cells treated as in (A) and stimulated with 10 μg/ml anti-IgM ($n = 5$, in duplicate). (**E**) Underflow adhesion on ICAM-1 of cells treated with DMSO (Control), TAT, or TAT-ICD (1 μM) for 1 h at 37°C ($n = 4$). (**F**) Underflow adhesion on VCAM-1 of cells treated as in (E) ($n = 4$). (**G**) LFA-1 low-intermediate affinity measurement of cells treated as in (E) and stimulated with 500 nM CXCL12 ($n = 3$). Shown are the percentages of fold increase over NT. (**H**) Histograms of fluorescence of a representative experiment of LFA-1 low-intermediate affinity. (**I**) LFA-1 high-affinity measurement of cells treated and stimulated as in (E) ($n = 3$). Shown are the percentages of fold increase over NT. (**J**) Histograms of fluorescence of a representative experiment of LFA-1 high affinity. (**K**) JAK2 activation assay in cells treated and then stimulated as in (E) ($n = 5$, in duplicate). (**L**) BTK activation assay in cells treated and stimulated as in (E) ($n = 5$). Shown are the percentages of fold increase over NT. (**M**) Histograms of fluorescence of a representative experiment of BTK activation. (**N**) RhoA activation of cells treated and stimulated as in (E) ($n = 5$ in duplicate). All data are expressed as mean ± SD. *$p < 0.05$, **$p < 0.01$ versus TAT.

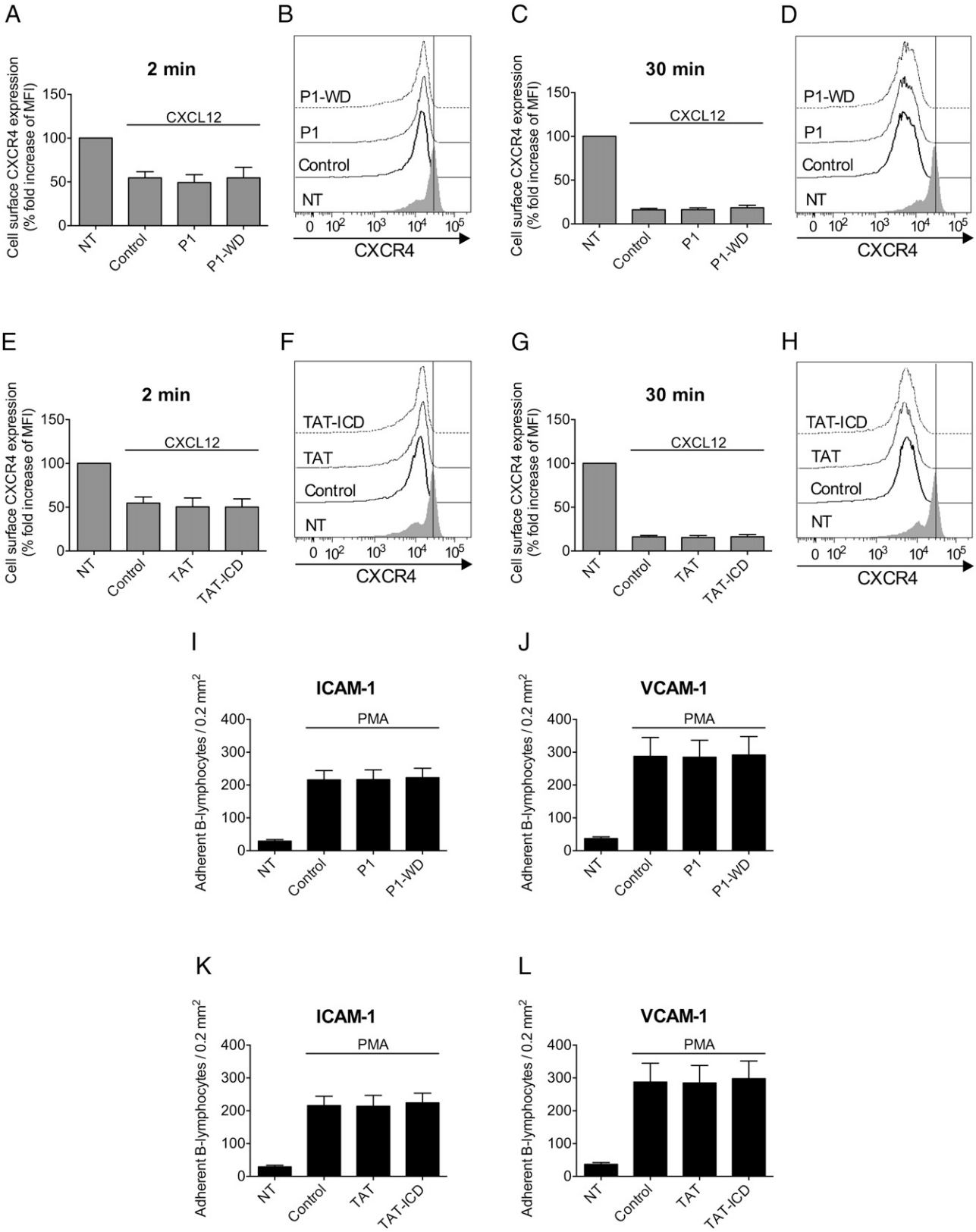

FIGURE 5. CXCR4 cell surface levels and PMA-induced adhesion are independent of PTPRG activity in CLL B lymphocytes. (**A** and **C**) CXCR4 cell surface expression in cells treated with DMSO (not treated [NT] and Control), P1, or P1-WD (50 μM) for 1 h at 37°C and then stimulated with 500 nM CXCL12 for the indicated times ($n = 4$). Shown are the percentages of fold increase over NT. (**B** and **D**) Histograms of fluorescence of a representative experiment of CXCR4 cell surface expression. (**E** and **G**) CXCR4 cell surface expression in cells treated with DMSO (NT and Control), TAT, or TAT-ICD (1 μM) for 1 h at 37°C and then stimulated with 500 nM CXCL12 for the indicated times ($n = 4$). Shown are the percentages of fold increase over NT. (**F** and **H**) Histograms of fluorescence of a representative experiment of CXCR4 cell surface expression. (**I** and **J**) Static adhesion on ICAM-1 or VCAM-1 of cells treated as in (A) and stimulated with 50 ng/ml PMA ($n = 5$, in duplicate). (**K** and **L**) Static adhesion on ICAM-1 or VCAM-1 of cells treated as in (E) and stimulated with 50 ng/ml PMA ($n = 4$, in duplicate). All data are expressed as mean ± SD. No statistically relevant differences were detected in P1 versus P1-WD or TAT versus TAT-ICD conditions.

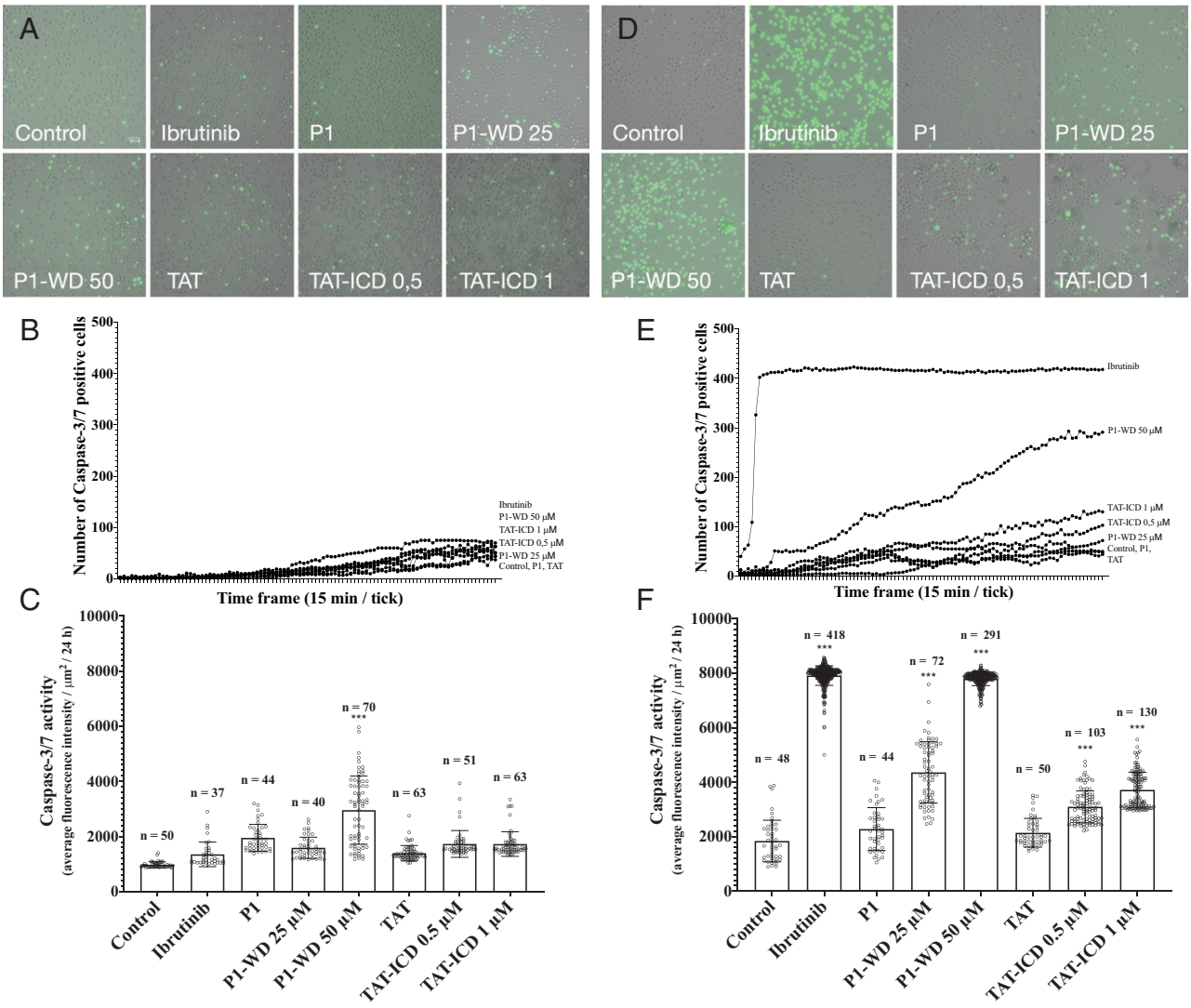

FIGURE 6. Activated PTPRG triggers robust apoptosis in CLL cells, but not in healthy B lymphocytes. (**A**) Superimposed bright-field and fluorescence photomicrographs of caspase-3/7–positive healthy B lymphocytes treated with DMSO (Control), 1 μM ibrutinib, 50 μM P1, 25 or 50 μM P1-WD, 1 μM TAT, and 0.5 or 1 μM TAT-ICD. (**B**) Kinetics of triggered apoptosis in healthy B lymphocytes. Shown is the number of caspase-3/7–positive cells detected every 15 min for 24 h; cells are treated as in (A). (**C**) Triggered apoptosis at 24 h in healthy B lymphocytes; cells are treated as in (A). Shown is the fluorescence intensity per micrometers squared, columns are average values, and small circles are individually analyzed cells showing the overall distribution of caspase-3/7 positivity. *n* = number of caspase-3/7–positive healthy B lymphocytes. (**D**) Superimposed bright-field and fluorescence photomicrographs of caspase-3/7–positive CLL cells treated with DMSO (Control), 1 μM ibrutinib, 50 μM P1, 25 or 50 μM P1-WD, 1 μM TAT, and 0.5 or 1 μM TAT-ICD. (**E**) Kinetics of triggered apoptosis in CLL cells. Shown is the number of caspase-3/7–positive cells calculated every 15 min for 24 h; cells are treated as in (D). (**F**) Triggered apoptosis at 24 h in CLL cells; cells are treated as in (D). Shown is the fluorescence intensity per micrometer squared, columns are average values, and small circles are individually analyzed cells, showing the overall distribution of caspase-3/7 positivity. *n* = number of caspase-3/7–positive CLL cells. Representative experiment of three. Average data are expressed as mean ± SD. ***$p < 0.001$ versus control, P1, or TAT.

to trigger effective apoptosis (Fig. 6A, 6B). Accordingly, quantitative end point analysis at 24 h showed that only the highest concentration of P1-WD triggered a rather modest increase of caspase-3/7 activity in a small number of cells (Fig. 6C).

In sharp contrast, in CLL cells, with respect to untreated cells, ibrutinib triggered a very rapid and consistent increase of the number of apoptotic cells. Moreover, when compared with the control P1 peptide, the PTPRG-activating P1-WD peptide triggered in a dose-dependent manner fast and robust apoptosis (Fig. 6D, 6E). Particularly, although slower than ibrutinib, P1-WD started to trigger apoptosis within 2 h. The data were confirmed with TAT-ICD. When compared to control TAT peptide, TAT-ICD triggered apoptosis in a dose-dependent manner, although to an extent lower than P1-WD. End point quantitative analysis at 24 h showed that although ibrutinib triggered apoptosis in a higher number of cells, the apoptosis strength, measured as caspase-3/7 activity, triggered by P1-WD and ibrutinib were identical, showing an overlapping intensity distribution of caspase-3/7–positive cells (Fig. 6F). Consistently, TAT-ICD also increased in a dose-dependent manner the number of apoptotic cells and the caspase-3/7 activity. Altogether, these data demonstrate, for the first time to our knowledge, that the triggering of PTPRG Tyr-phosphatase activity selectively induces robust apoptosis in CLL cells, but not in healthy B lymphocytes, thus highlighting the specific negative regulatory role of PTPRG on CLL cell survival.

PTPRG-triggered apoptosis is weakly sensitive to survival signals generated by CXCR4 and BCR

We finally tested whether PTPRG-triggered apoptosis in CLL cells could be affected by prosurvival signals generated by stromal

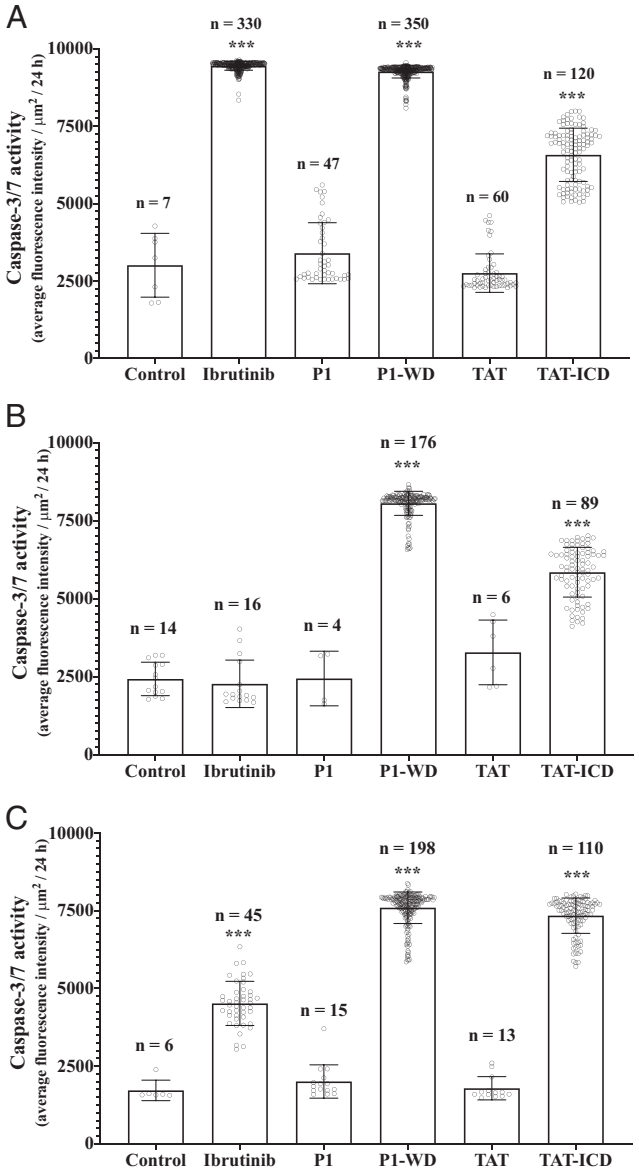

FIGURE 7. PTPRG-triggered apoptosis is insensitive to signals from CXCR4 and BCR. Shown is triggered apoptosis at 24 h in CLL cells treated with DMSO (Control), 1 μM ibrutinib, 50 μM P1, 50 μM P1-WD, 1 μM TAT, and 1 μM TAT-ICD. Cells were concurrently treated with buffer (**A**), 500 nM CXCL12 (**B**), or 10 μg/ml anti-IgM (**C**). Shown is the fluorescence intensity per micrometer squared, columns are average values, and small circles are individually analyzed cells, showing the overall distribution of caspase-3/7 positivity. *n* = number of caspase-3/7–positive CLL cells. Representative experiment of four. Average data are expressed as mean ± SD. ***$p < 0.001$ versus control, P1, or TAT.

factors. To this end, CLL cells were treated with PTPRG-activating CPPs in the presence of CXCL12 or anti-IgM to trigger, concurrently with PTPRG signaling, CXCR4 and BCR signals. As shown in Fig. 7A, and in accordance with the above data, ibrutinib, P1-WD, and TAT-ICD triggered robust apoptosis in CLL cells in absence of CXCL12 or anti-IgM. However, in the presence of CXCL12 (Fig. 7B) or anti-IgM (Fig. 7C), the capability of ibrutinib to trigger apoptosis was strongly suppressed, either considering the number of apoptotic cells (−95% in the presence of CXCL12 and −77% in the presence of anti-IgM) or the average intensity of caspase-3/7 activity (−76% in the presence of CXCL12 and −53% in the presence of anti-IgM). In contrast, the capability of P1-WD to trigger apoptosis was much less affected by CXCL12 (Fig. 7B) or anti-IgM (Fig. 7C) signals, with −50% and −44% of the number of apoptotic cells and −13% and −18% of the average intensity of caspase-3/7 activity, respectively. Finally, the capability of TAT-ICD to trigger apoptosis was even less affected by CXCL12 (Fig. 7B) or anti-IgM (Fig. 7C) signals, with −26% and −9% of the number of apoptotic cells and −12% and 9% of the average intensity of caspase-3/7 activity, respectively.

Altogether, these data show that, in contrast to ibrutinib, PTPRG-triggered apoptosis in CLL cells is, overall, poorly contrasted by prosurvival signals generated by CXCR4 and BCR.

Discussion

CLL is characterized by a landscape of genetic alterations leading to the emergence of a heterogenous disease spanning from almost indolent to very aggressive, therapy-resistant manifestations (38–40). The molecular mechanisms underlying CLL pathogenesis are not fully understood. Much evidence points to the importance of the stromal microenvironment and chemokine-regulated integrin activation in CLL pathogenesis and progression, leading to prolonged cell survival and exacerbated dissemination (41–45).

In recent years, combined chemoimmunotherapy has been shown to be an effective therapeutic regimen for CLL, although its efficacy was limited by comorbidities and fitness of the patients (46–51). Treatment with specific inhibitors of signaling mechanisms is thus progressively replacing chemoimmunotherapy, greatly improving the therapeutic efficacy. Ibrutinib for BTK, idelalisib for PI3K (isoform p110δ), and venetoclax for BCL-2 are examples of targeted therapies for which adoption is going to revolutionize CLL therapy (52–56). Nevertheless, these targeted treatments may also eventually fail. For instance, in CLL relapse after ibrutinib treatment, ∼67% of patients present the BTK C481S point mutation, making BTK insensitive to ibrutinib; moreover, 6% of patients show PLCG2 mutation, and 13% show combined BTK/PLCG2 mutations (57). Notably, PLCG2, a direct BTK effector, prevalently presents gain-of-function mutations, thus leading to downstream pathway activation even in regimens of BTK inhibition (58). Moreover, even if resistance to idelalisib has not yet been fully characterized, it was reported that upregulation of either *PI3KCD* or alternative class 1A PI3K, such as *PI3KCA* or *PI3KCB*, can occur, negatively affecting idelalisib efficacy (59). For venetoclax, mechanisms of resistance are not yet reported, but a possible cause of resistance could be the upregulation of a different member of the BCL-2 family, such as BCL-W, BCL-XL, or MCL1 (60, 61). Overall, monotargeted therapies may eventually favor the emergence of drug-resistant clones. This is clearly exemplified by Richter syndrome (RS), which represents the most severe CLL evolution (62). RS has a poor prognosis, which becomes even worse in patients who transformed on previous therapies, such as ibrutinib. Indeed, BTK or PLCG2 mutations account for most of the ibrutinib-resistant CLL progressions to RS (63, 64). Thus, although representing the front line in CLL treatment, the new therapeutic regimens, based on highly selective compounds, may potentially lead to clonal selection, thus increasing the incidence of progression to a more aggressive disease. It is therefore imperative to deepen the knowledge of signaling mechanisms regulating CLL pathogenesis to envision new therapeutic strategies.

In this study, we investigated whether integrin-mediated adhesion and survival of leukemic cells isolated from patients with CLL could be hampered by the specific activation of protein Tyr-

phosphatases. We focused on PTPRG because it is a tumor suppressor gene (65), and it was shown to possess the highest intrinsic Tyr-phosphatase activity among all human phosphatases and the highest tendency to generate homodimers devoid of enzymatic activity (29), thus suggesting that PTPRG is an ideal target of activation by means of controlled monomerization (27, 66, 67). As no direct mechanisms of PTPRG activation by agonists or natural ligands have been described in literature, we have previously developed a dual approach based on CPPs to study PTPRG signaling in primary cells (27). The first approach targets the intracellular juxta-membrane regulatory region called WD involved in stabilizing the inactive homodimeric conformation of PTPRG. A P1-WD fusion peptide was developed capable of disrupting, by steric hindrance, the WD-mediated PTPRG homodimerization, thus freeing the intrinsic phosphatase activity of PTPRG ICD. As a second complementary approach, we generated a TAT fusion protein encompassing the complete, enzymatically active, PTPRG ICD (TAT-ICD), retaining full Tyr-phosphatase activity.

We found that activation of PTPRG strongly prevents β_1- and β_2-integrin triggering by CXCR4 and BCR. Importantly, signaling analysis showed that JAK2, BTK, and RhoA, all central to integrin activation, are inhibited by PTPRG activity. Importantly, P1-WD and TAT-ICD worked equally well in healthy as well as CLL B cells, thus suggesting that in CLL cells, PTPRG is normally modulated by homodimerization and, once in a monomeric state, becomes fully functional. Notably, CXCL12-triggered downmodulation of CXCR4 expression and PMA-induced integrin activation are not affected by PTPRG activation. These data show, for the first time to our knowledge, that PTPRG is a negative regulator of signaling events specifically controlling integrin activation in CLL cells, thus suggesting that PTPRG activity could interfere with the dissemination of CLL cells.

Furthermore, we found that PTPRG activation specifically triggers strong apoptosis in CLL cells. Interestingly, although ibrutinib triggered apoptosis more rapidly and in a higher number of cells, quantification at 24 h showed that the intensity of P1-WD–triggered apoptosis, measured as caspase-3/7 activity, as well as the intensity distribution of apoptotic cell were identical to those of ibrutinib. The data were also confirmed with TAT-ICD, with the observed quantitative differences likely reflecting the different intracellular diffusion rate and/or the different modality of action of the two CPPs (27). Overall, these data show that PTPRG activation is as effective as ibrutinib in triggering specific apoptosis in leukemic cells isolated from patients with CLL. However, we observed an important difference. Indeed, ibrutinib induced an effective apoptosis only in absence of concurrent CXCR4- or BCR-triggered signals. In contrast, PTPRG did trigger effective apoptosis also in the presence of CXCR4- or BCR-triggered signaling. Thus, stromal factors can counteract ibrutinib- but not PTPRG-induced apoptosis. This is an interesting observation because it may suggest that PTPRG could also induce apoptosis in CLL cells surrounded by a protective stromal environment. This difference could reflect the different impact ibrutinib and PTPRG may have on signaling mechanisms. Indeed, ibrutinib is a BTK inhibitor, whereas, in contrast, we previously showed that at least 31 signaling molecules are targets of PTPRG modulation of Tyr-phosphorylation (27, 66, 67), including BTK and JAK PTKs. Thus, activation of PTPRG could possibly have a broader effect on signaling mechanisms, more difficult to compensate for by stromal factors or by cancer progression. As we stated above, BTK activation by chemokines is mediated by JAK2 (24). Notably, JAK2 inhibition was shown to trigger apoptosis in CLL cells (68). Thus, a PTPRG-targeted approach could be potentially highly effective in CLL; indeed, being both JAK and BTK PTPRG targets, the effect of BTK mutations determining resistance to ibrutinib could be bypassed by the direct inhibitory effect of PTPRG. In this context, it will be of great interest to test whether PTPRG activation may trigger apoptosis in patients with CLL resistant to ibrutinib.

Notably, PTPRG is equally expressed in both healthy and CLL B cells. However, PTPRG activation triggers apoptosis only in CLL cells. Thus, although it is possible that our data may not entirely recapitulate the normal physiological function of PTPRG, especially considering that no physiological activators of PTPRG are known; nevertheless, activated PTPRG seems to be arising as a potential Achilles' heel of CLL cells. Interestingly, PTPROt, a PTPRG-related Tyr-phosphatase, has recently been suggested to be a tumor suppressor gene in CLL (17). Moreover, a study was recently published showing that a small compound leading to upmodulation of the phosphatase activity of SHIP1 may induce inhibition of BCR-mediated PI3K and AKT activation and caspase-mediated apoptosis in CLL cells (20). Altogether, these data clearly suggest that activation of specific phosphatases may prevent the course of CLL pathogenesis.

The logic of our dual CPP-based methodology is perfectly in keeping with the SHIP1 activation approach (20) and suggests that unleashing the PTPRG enzymatic activity may represent an innovative approach to CLL treatment, possibly circumventing the limitations of monotargeted therapies. Because our approach based on CPPs was developed mainly to test a scientific rationale, an important step forward will be to develop, as for SHIP1, small compound activators of PTPRG, possibly mimicking the steric hindrance capability of P1-WD. Notably, recent data (69, 70) suggest that a cyclic structure could improve our P1-WD peptide in term of stability and in vivo efficacy. It will be of interest to investigate these possibilities in our context.

Acknowledgments

We thank Prof. C. Sorio (Department of Medicine, University of Verona) for kindly providing the anti-PTPRG antibody (TPγ B9-2 clone).

Disclosures

The authors have no financial conflicts of interest.

References

1. Pangalis, G. A., T. P. Vassilakopoulos, M. N. Dimopoulou, M. P. Siakantaris, F. N. Kontopidou, and M. K. Angelopoulou. 2002. B-chronic lymphocytic leukemia: practical aspects. *Hematol. Oncol.* 20: 103–146.
2. Möhle, R., C. Failenschmid, F. Bautz, and L. Kanz. 1999. Overexpression of the chemokine receptor CXCR4 in B cell chronic lymphocytic leukemia is associated with increased functional response to stromal cell-derived factor-1 (SDF-1). *Leukemia* 13: 1954–1959.
3. Bulian, P., T. D. Shanafelt, C. Fegan, A. Zucchetto, L. Cro, H. Nückel, L. Baldini, A. V. Kurtova, A. Ferrajoli, J. A. Burger, et al. 2014. CD49d is the strongest flow cytometry-based predictor of overall survival in chronic lymphocytic leukemia. *J. Clin. Oncol.* 32: 897–904.
4. Ponader, S., S. S. Chen, J. J. Buggy, K. Balakrishnan, V. Gandhi, W. G. Wierda, M. J. Keating, S. O'Brien, N. Chiorazzi, and J. A. Burger. 2012. The Bruton tyrosine kinase inhibitor PCI-32765 thwarts chronic lymphocytic leukemia cell survival and tissue homing in vitro and in vivo. *Blood* 119: 1182–1189.
5. de Rooij, M. F., A. Kuil, C. R. Geest, E. Eldering, B. Y. Chang, J. J. Buggy, S. T. Pals, and M. Spaargaren. 2012. The clinically active BTK inhibitor PCI-32765 targets B-cell receptor- and chemokine-controlled adhesion and migration in chronic lymphocytic leukemia. *Blood* 119: 2590–2594.
6. Cheng, S., J. Ma, A. Guo, P. Lu, J. P. Leonard, M. Coleman, M. Liu, J. J. Buggy, R. R. Furman, and Y. L. Wang. 2014. BTK inhibition targets in vivo CLL proliferation through its effects on B-cell receptor signaling activity. *Leukemia* 28: 649–657.
7. Takata, M., and T. Kurosaki. 1996. A role for Bruton's tyrosine kinase in B cell antigen receptor-mediated activation of phospholipase C-gamma 2. *J. Exp. Med.* 184: 31–40.
8. Watanabe, D., S. Hashimoto, M. Ishiai, M. Matsushita, Y. Baba, T. Kishimoto, T. Kurosaki, and S. Tsukada. 2001. Four tyrosine residues in phospholipase C-gamma 2, identified as Btk-dependent phosphorylation sites, are required for B cell antigen receptor-coupled calcium signaling. *J. Biol. Chem.* 276: 38595–38601.
9. Abrams, S. T., T. Lakum, K. Lin, G. M. Jones, A. T. Treweeke, M. Farahani, M. Hughes, M. Zuzel, and J. R. Slupsky. 2007. B-cell receptor signaling in chronic

lymphocytic leukemia cells is regulated by overexpressed active protein kinase CbetaII. *Blood* 109: 1193–1201.
10. Hashimoto, A., H. Okada, A. Jiang, M. Kurosaki, S. Greenberg, E. A. Clark, and T. Kurosaki. 1998. Involvement of guanosine triphosphatases and phospholipase C-gamma2 in extracellular signal-regulated kinase, c-Jun NH2-terminal kinase, and p38 mitogen-activated protein kinase activation by the B cell antigen receptor. *J. Exp. Med.* 188: 1287–1295.
11. Saijo, K., I. Mecklenbräuker, A. Santana, M. Leitger, C. Schmedt, and A. Tarakhovsky. 2002. Protein kinase C beta controls nuclear factor kappaB activation in B cells through selective regulation of the IkappaB kinase alpha. *J. Exp. Med.* 195: 1647–1652.
12. Volmering, S., H. Block, M. Boras, C. A. Lowell, and A. Zarbock. 2016. The neutrophil Btk signalosome regulates integrin activation during sterile inflammation. *Immunity* 44: 73–87.
13. Tsukada, S., M. I. Simon, O. N. Witte, and A. Katz. 1994. Binding of beta gamma subunits of heterotrimeric G proteins to the PH domain of Bruton tyrosine kinase. *Proc. Natl. Acad. Sci. USA* 91: 11256–11260.
14. Lowry, W. E., and X. Y. Huang. 2002. G Protein beta gamma subunits act on the catalytic domain to stimulate Bruton's agammaglobulinemia tyrosine kinase. *J. Biol. Chem.* 277: 1488–1492.
15. Hendriks, R. W., S. Yuvaraj, and L. P. Kil. 2014. Targeting Bruton's tyrosine kinase in B cell malignancies. *Nat. Rev. Cancer* 14: 219–232.
16. de Gorter, D. J., E. A. Beuling, R. Kersseboom, S. Middendorp, J. M. van Gils, R. W. Hendriks, S. T. Pals, and M. Spaargaren. 2007. Bruton's tyrosine kinase and phospholipase Cgamma2 mediate chemokine-controlled B cell migration and homing. *Immunity* 26: 93–104.
17. Wakim, J., E. Arman, S. Becker-Herman, M. P. Kramer, E. Bakos, I. Shachar, and A. Elson. 2017. The PTPROt tyrosine phosphatase functions as an obligate haploinsufficient tumor suppressor in vivo in B-cell chronic lymphocytic leukemia. *Oncogene* 36: 3686–3694.
18. O'Hayre, M., M. Niederst, J. F. Fecteau, V. M. Nguyen, T. J. Kipps, D. Messmer, A. C. Newton, and T. M. Handel. 2012. Mechanisms and consequences of the loss of PHLPP1 phosphatase in chronic lymphocytic leukemia (CLL). *Leukemia* 26: 1689–1692.
19. Beke Debreceni, I., R. Szász, Z. Kónya, F. Erdődi, F. Kiss, and J. Kappelmayer. 2019. L-Selectin expression is influenced by phosphatase activity in chronic lymphocytic leukemia. *Cytometry B Clin. Cytom.* 96: 149–157.
20. Lemm, E. A., B. Valle-Argos, L. D. Smith, J. Richter, Y. Gebreselassie, M. J. Carter, J. Karolova, M. Svaton, K. Helman, N. J. Weston-Bell, et al. 2020. Preclinical evaluation of a novel SHIP1 phosphatase activator for inhibition of PI3K signaling in malignant B cells. *Clin. Cancer Res.* 26: 1700–1711.
21. Pal Singh, S., M. J. W. de Bruijn, C. Velaso Gago da Graça, O. B. J. Corneth, J. Rip, R. Stadhouders, R. W. J. Meijers, S. Schurmans, W. G. Kerr, J. Ter Burg, et al. 2020. Overexpression of SH2-containing inositol phosphatase contributes to chronic lymphocytic leukemia survival. *J. Immunol.* 204: 360–374.
22. Montresor, A., L. Toffali, G. Constantin, and C. Laudanna. 2012. Chemokines and the signaling modules regulating integrin affinity. *Front. Immunol.* 3: 127.
23. Montresor, A., L. Toffali, M. Mirenda, A. Rigo, F. Vinante, and C. Laudanna. 2015. JAK2 tyrosine kinase mediates integrin activation induced by CXCL12 in B-cell chronic lymphocytic leukemia. *Oncotarget* 6: 34245–34257.
24. Montresor, A., L. Toffali, A. Rigo, I. Ferrarini, F. Vinante, and C. Laudanna. 2018. CXCR4- and BCR-triggered integrin activation in B-cell chronic lymphocytic leukemia cells depends on JAK2-activated Bruton's tyrosine kinase. *Oncotarget* 9: 35123–35140.
25. Tonks, N. K. 2006. Protein tyrosine phosphatases: from genes, to function, to disease. *Nat. Rev. Mol. Cell Biol.* 7: 833–846.
26. Tonks, N. K. 2013. Protein tyrosine phosphatases–from housekeeping enzymes to master regulators of signal transduction. *FEBS J.* 280: 346–378.
27. Mirenda, M., L. Toffali, A. Montresor, G. Scardoni, C. Sorio, and C. Laudanna. 2015. Protein tyrosine phosphatase receptor type γ is a JAK phosphatase and negatively regulates leukocyte integrin activation. *J. Immunol.* 194: 2168–2179.
28. Vezzalini, M., A. Mafficini, L. Tomasello, E. Lorenzetto, E. Moratti, Z. Fiorini, T. L. Holyoake, F. Pellicano, M. Krampera, C. Tecchio, et al. 2017. A new monoclonal antibody detects downregulation of protein tyrosine phosphatase receptor type γ in chronic myeloid leukemia patients. *J. Hematol. Oncol.* 10: 129.
29. Barr, A. J., E. Ugochukwu, W. H. Lee, O. N. King, P. Filippakopoulos, I. Alfano, P. Savitsky, N. A. Burgess-Brown, S. Müller, and S. Knapp. 2009. Large-scale structural analysis of the classical human protein tyrosine phosphatome. *Cell* 136: 352–363.
30. Gilbert, C., S. Levasseur, P. Desaulniers, A. A. Dusseault, N. Thibault, S. G. Bourgoin, and P. H. Naccache. 2003. Chemotactic factor-induced recruitment and activation of Tec family kinases in human neutrophils. II. Effects of LFM-A13, a specific Btk inhibitor. *J. Immunol.* 170: 5235–5243.
31. Mangla, A., A. Khare, V. Vineeth, N. N. Panday, A. Mukhopadhyay, B. Ravindran, V. Bal, A. George, and S. Rath. 2004. Pleiotropic consequences of Bruton tyrosine kinase deficiency in myeloid lineages lead to poor inflammatory responses. *Blood* 104: 1191–1197.
32. Honda, F., H. Kano, H. Kanegane, S. Nonoyama, E. S. Kim, S. K. Lee, M. Takagi, S. Mizutani, and T. Morio. 2012. The kinase Btk negatively regulates the production of reactive oxygen species and stimulation-induced apoptosis in human neutrophils. *Nat. Immunol.* 13: 369–378.
33. Burger, J. A., N. Tsukada, M. Burger, N. J. Zvaifler, M. Dell'Aquila, and T. J. Kipps. 2000. Blood-derived nurse-like cells protect chronic lymphocytic leukemia B cells from spontaneous apoptosis through stromal cell-derived factor-1. *Blood* 96: 2655–2663.
34. Burger, M., T. Hartmann, M. Krome, J. Rawluk, H. Tamamura, N. Fujii, T. J. Kipps, and J. A. Burger. 2005. Small peptide inhibitors of the CXCR4 chemokine receptor (CD184) antagonize the activation, migration, and antiapoptotic responses of CXCL12 in chronic lymphocytic leukemia B cells. *Blood* 106: 1824–1830.
35. Bernal, A., R. D. Pastore, Z. Asgary, S. A. Keller, E. Cesarman, H. C. Liou, and E. J. Schattner. 2001. Survival of leukemic B cells promoted by engagement of the antigen receptor. *Blood* 98: 3050–3057.
36. Ten Hacken, E., M. Sivina, E. Kim, S. O'Brien, W. G. Wierda, A. Ferrajoli, Z. Estrov, M. J. Keating, T. Oellerich, C. Scielzo, et al. 2016. Functional differences between IgM and IgD signaling in chronic lymphocytic leukemia. *J. Immunol.* 197: 2522–2531.
37. Dubois, N., E. Crompot, N. Meuleman, D. Bron, L. Lagneaux, and B. Stamatopoulos. 2020. Importance of crosstalk between chronic lymphocytic leukemia cells and the stromal microenvironment: direct contact, soluble factors, and extracellular vesicles. *Front. Oncol.* 10: 1422.
38. Puente, X. S., M. Pinyol, V. Quesada, L. Conde, G. R. Ordóñez, N. Villamor, G. Escaramis, P. Jares, S. Beà, M. González-Díaz, et al. 2011. Whole-genome sequencing identifies recurrent mutations in chronic lymphocytic leukaemia. *Nature* 475: 101–105.
39. Landau, D. A., E. Tausch, A. N. Taylor-Weiner, C. Stewart, J. G. Reiter, J. Bahlo, S. Kluth, I. Bozic, M. Lawrence, S. Böttcher, et al. 2015. Mutations driving CLL and their evolution in progression and relapse. *Nature* 526: 525–530.
40. Gaidano, G., and D. Rossi. 2017. The mutational landscape of chronic lymphocytic leukemia and its impact on prognosis and treatment. *Hematology (Am. Soc. Hematol. Educ. Program)* 2017: 329–337.
41. Oppezzo, P., and G. Dighiero. 2013. "Role of the B-cell receptor and the microenvironment in chronic lymphocytic leukemia". *Blood Cancer J.* 3: e149.
42. Burger, J. A., and J. G. Gribben. 2014. The microenvironment in chronic lymphocytic leukemia (CLL) and other B cell malignancies: insight into disease biology and new targeted therapies. *Semin. Cancer Biol.* 24: 71–81.
43. Ten Hacken, E., and J. A. Burger. 2016. Microenvironment interactions and B-cell receptor signaling in chronic lymphocytic leukemia: Implications for disease pathogenesis and treatment. *Biochim. Biophys. Acta* 1863: 401–413.
44. Choi, M. Y., M. K. Kashyap, and D. Kumar. 2016. The chronic lymphocytic leukemia microenvironment: beyond the B-cell receptor. *Best Pract. Res. Clin. Haematol.* 29: 40–53.
45. Guo, A., P. Lu, G. Coffey, P. Conley, A. Pandey, and Y. L. Wang. 2017. Dual SYK/JAK inhibition overcomes ibrutinib resistance in chronic lymphocytic leukemia: Cerdulatinib, but not ibrutinib, induces apoptosis of tumor cells protected by the microenvironment. *Oncotarget* 8: 12953–12967.
46. Hallek, M., K. Fischer, G. Fingerle-Rowson, A. M. Fink, R. Busch, J. Mayer, M. Hensel, G. Hopfinger, G. Hess, U. von Grünhagen, et al; German Chronic Lymphocytic Leukaemia Study Group. 2010. Addition of rituximab to fludarabine and cyclophosphamide in patients with chronic lymphocytic leukaemia: a randomised, open-label, phase 3 trial. *Lancet* 376: 1164–1174.
47. Robak, T., A. Dmoszynska, P. Solal-Céligny, K. Warzocha, J. Loscertales, J. Catalano, B. V. Afanasiev, L. Larratt, C. H. Geisler, M. Montillo, et al. 2010. Rituximab plus fludarabine and cyclophosphamide prolongs progression-free survival compared with fludarabine and cyclophosphamide alone in previously treated chronic lymphocytic leukemia. *J. Clin. Oncol.* 28: 1756–1765.
48. Fischer, K., P. Cramer, R. Busch, S. Böttcher, J. Bahlo, J. Schubert, K. H. Pflüger, S. Schott, V. Goede, S. Isfort, et al. 2012. Bendamustine in combination with rituximab for previously untreated patients with chronic lymphocytic leukemia: a multicenter phase II trial of the German Chronic Lymphocytic Leukemia Study Group. *J. Clin. Oncol.* 30: 3209–3216.
49. Baumann, T., J. Delgado, R. Santacruz, A. Martínez-Trillos, C. Royo, A. Navarro, M. Pinyol, M. Rozman, A. Pereira, N. Villamor, et al. 2014. Chronic lymphocytic leukemia in the elderly: clinico-biological features, outcomes, and proposal of a prognostic model. *Haematologica* 99: 1599–1604.
50. Goede, V., K. Fischer, R. Busch, A. Engelke, B. Eichhorst, C. M. Wendtner, T. Chagorova, J. de la Serna, M. S. Dilhuydy, T. Illmer, et al. 2014. Obinutuzumab plus chlorambucil in patients with CLL and coexisting conditions. *N. Engl. J. Med.* 370: 1101–1110.
51. Eichhorst, B., A. M. Fink, J. Bahlo, R. Busch, G. Kovacs, C. Maurer, E. Lange, H. Köppler, M. Kiehl, M. Sökler, et al; German CLL Study Group (GCLLSG). 2016. First-line chemoimmunotherapy with bendamustine and rituximab versus fludarabine, cyclophosphamide, and rituximab in patients with advanced chronic lymphocytic leukaemia (CLL10): an international, open-label, randomised, phase 3, non-inferiority trial. *Lancet Oncol.* 17: 928–942.
52. Byrd, J. C., R. R. Furman, S. E. Coutre, I. W. Flinn, J. A. Burger, K. A. Blum, B. Grant, J. P. Sharman, M. Coleman, W. G. Wierda, et al. 2013. Targeting BTK with ibrutinib in relapsed chronic lymphocytic leukemia. *N. Engl. J. Med.* 369: 32–42.
53. Furman, R. R., J. P. Sharman, S. E. Coutre, B. D. Cheson, J. M. Pagel, P. Hillmen, J. C. Barrientos, A. D. Zelenetz, T. J. Kipps, I. Flinn, et al. 2014. Idelalisib and rituximab in relapsed chronic lymphocytic leukemia. *N. Engl. J. Med.* 370: 997–1007.
54. Burger, J. A., A. Tedeschi, P. M. Barr, T. Robak, C. Owen, P. Ghia, O. Bairey, P. Hillmen, N. L. Bartlett, J. Li, et al; RESONATE-2 Investigators. 2015. Ibrutinib as Initial Therapy for Patients with Chronic Lymphocytic Leukemia. *N. Engl. J. Med.* 373: 2425–2437.
55. O'Brien, S., J. A. Jones, S. E. Coutre, A. R. Mato, P. Hillmen, C. Tam, A. Österborg, T. Siddiqi, M. J. Thirman, R. R. Furman, et al. 2016. Ibrutinib for patients with relapsed or refractory chronic lymphocytic leukaemia with 17p deletion (RESONATE-17): a phase 2, open-label, multicentre study. *Lancet Oncol.* 17: 1409–1418.
56. Roberts, A. W., M. S. Davids, J. M. Pagel, B. S. Kahl, S. D. Puvvada, J. F. Gerecitano, T. J. Kipps, M. A. Anderson, J. R. Brown, L. Gressick, et al. 2016. Targeting BCL2 with venetoclax in relapsed chronic lymphocytic leukemia. *N. Engl. J. Med.* 374: 311–322.
57. Woyach, J. A., A. S. Ruppert, D. Guinn, A. Lehman, J. S. Blachly, A. Lozanski, N. A. Heerema, W. Zhao, J. Coleman, D. Jones, et al. 2017. BTK^{C481S}-mediated resistance to ibrutinib in chronic lymphocytic leukemia. *J. Clin. Oncol.* 35: 1437–1443.

58. Liu, T. M., J. A. Woyach, Y. Zhong, A. Lozanski, G. Lozanski, S. Dong, E. Strattan, A. Lehman, X. Zhang, J. A. Jones, et al. 2015. Hypermorphic mutation of phospholipase C, γ2 acquired in ibrutinib-resistant CLL confers BTK independency upon B-cell receptor activation. *Blood* 126: 61–68.
59. Iyengar, S., A. Clear, C. Bödör, L. Maharaj, A. Lee, M. Calaminici, J. Matthews, S. Iqbal, R. Auer, J. Gribben, and S. Joel. 2013. P110α-mediated constitutive PI3K signaling limits the efficacy of p110δ-selective inhibition in mantle cell lymphoma, particularly with multiple relapse. *Blood* 121: 2274–2284.
60. Youle, R. J., and A. Strasser. 2008. The BCL-2 protein family: opposing activities that mediate cell death. *Nat. Rev. Mol. Cell Biol.* 9: 47–59.
61. Vogler, M., M. Butterworth, A. Majid, R. J. Walewska, X. M. Sun, M. J. Dyer, and G. M. Cohen. 2009. Concurrent up-regulation of BCL-XL and BCL2A1 induces approximately 1000-fold resistance to ABT-737 in chronic lymphocytic leukemia. *Blood* 113: 4403–4413.
62. Jain, N., and M. J. Keating. 2016. Richter transformation of CLL. *Expert Rev. Hematol.* 9: 793–801.
63. Kadri, S., J. Lee, C. Fitzpatrick, N. Galanina, M. Sukhanova, G. Venkataraman, S. Sharma, B. Long, K. Petras, M. Theissen, et al. 2017. Clonal evolution underlying leukemia progression and Richter transformation in patients with ibrutinib-relapsed CLL. *Blood Adv.* 1: 715–727.
64. Vaisitti, T., E. Braggio, J. N. Allan, F. Arruga, S. Serra, A. Zamò, W. Tam, A. Chadburn, R. R. Furman, and S. Deaglio. 2018. Novel Richter syndrome xenograft models to study genetic architecture, biology, and therapy responses. *Cancer Res.* 78: 3413–3420.
65. Della Peruta, M., G. Martinelli, E. Moratti, D. Pintani, M. Vezzalini, A. Mafficini, T. Grafone, I. Iacobucci, S. Soverini, M. Murineddu, et al. 2010. Protein tyrosine phosphatase receptor type gamma is a functional tumor suppressor gene specifically downregulated in chronic myeloid leukemia. *Cancer Res.* 70: 8896–8906.
66. Majeti, R., A. M. Bilwes, J. P. Noel, T. Hunter, and A. Weiss. 1998. Dimerization-induced inhibition of receptor protein tyrosine phosphatase function through an inhibitory wedge. *Science* 279: 88–91.
67. Jiang, G., J. den Hertog, J. Su, J. Noel, J. Sap, and T. Hunter. 1999. Dimerization inhibits the activity of receptor-like protein-tyrosine phosphatase-alpha. *Nature* 401: 606–610.
68. Severin, F., F. Frezzato, A. Visentin, V. Martini, V. Trimarco, S. Carraro, E. Tibaldi, A. M. Brunati, F. Piazza, G. Semenzato, et al. 2019. In chronic lymphocytic leukemia the JAK2/STAT3 pathway is constitutively activated and its inhibition leads to CLL cell death unaffected by the protective bone marrow microenvironment. *Cancers (Basel).* 11: 1939.
69. Gang, D., D. W. Kim, and H. S. Park. 2018. Cyclic peptides: promising scaffolds for biopharmaceuticals. *Genes (Basel)* 9: 557.
70. Tetley, G. J. N., N. P. Murphy, S. Bonetto, G. Ivanova-Berndt, J. Revell, H. R. Mott, R. N. Cooley, and D. Owen. 2020. The discovery and maturation of peptide biologics targeting the small G-protein Cdc42: A bioblockade for Ras-driven signaling. *J. Biol. Chem.* 295: 2866–2884.